Clays and Clay Minerals, Vol. 62, No. 2, 102–111, 2014.

STUDY OF LOW-PRESSURE ARGON ADSORPTION ON SYNTHETIC NONTRONITE: IMPLICATIONS FOR SMECTITE CRYSTAL GROWTH

ALAIN DECARREAU[1], SABINE PETIT[1,*], PAULINE ANDRIEUX[1], FREDERIC VILLIERAS[2], MANUEL PELLETIER[2], AND ANGELINA RAZAFITIANAMAHARAVO[2]

[1] Université de Poitiers, CNRS UMR 7285 IC2MP, HydrASA, 6 rue Michel Brunet, F-86022 Poitiers Cedex, France
[2] Laboratoire Environnement et Minéralurgie, UMR 7569, CNRS Université de Lorraine, BP 40, F-54501 Vandoeuvre-lès-Nancy, France

Abstract—Because relatively little information about the crystal-growth process of smectite is available, the process was assessed here by studying the size and shape of nontronite particles synthesized at six different temperatures from 75 to 150ºC over a period of 4 weeks.

The morphology of nontronites was studied using low-pressure isotherms of argon adsorption at 77 K, a method which enables the measurement of the basal and edge surface areas of the nontronite particles and of their mean diameter and thickness. During the crystal growth of nontronite, the mean particle length increased whereas their thickness (and the number of stacked layers) did not vary significantly.

A specific two-dimensional crystal-growth process was observed for smectite *via* the lateral extension of the layers. This process also appears to occur during the growth of neoformed natural smectite.

Key Words—Argon Adsorption, Crystal Growth, Crystallinity, Infrared Spectroscopy, Isotherm, Nontronite, Particle Size, Smectite, Surface Area, Synthesis.

INTRODUCTION

The most notable property of smectites, compared to other clay minerals, is the expandability of its layers, which is linked to the nature and number of polar molecules (water, glycol, *etc.*) that surround the interlayer cations (Brindley and Brown, 1980). The *c* crystallographic parameter is variable for layers with a constant chemistry. In smectite, the interlayer cations (*e.g.* Na^+, K^+, Li^+, Ca^{2+}, and Mg^{2+}) are exchangeable and depend on the composition of the last fluid that was in contact with the smectite. Thus, only the 2:1 layer is relatively stable with time, in contrast to the labile interlayer.

Smectites are generally described as thin crumpled sheets (with a few tens of stacked layers), a few hundred nanometers wide, usually anhedral, which form aggregates (Güven, 1988). The study of the morphological evolution of smectites during crystal growth in natural or experimental systems is not straightforward, therefore. Numerous studies of smectite synthesis exist in the literature (for examples see reviews by Kloprogge *et al*., 1999, and Zhang *et al*., 2010). In such studies, however, data on the shape and size of the smectite particles are often discussed with respect to synthesis conditions (temperature, pressure, pH, ...) and not with respect to the crystal-growth issue.

Transmission electron microscopy (TEM) and atomic force microscopy (AFM) are useful tools for studying the morphology of clays and many studies have been devoted to imaging in three dimensions clay minerals with euhedral or sub-euhedral character, such as kaolinite, micas, and mixed-layer clays (Meunier, 2010 and references therein). For these clay minerals, crystal growth occurs *via* three-dimensional processes and often exhibits polygonal and spiral-growth patterns (Baronnet, 1972; Meunier, 2010). Researchers have also used TEM and AFM to study smectite dissolution (*e.g*. Bickmore *et al*., 2001; Bauer *et al.*, 2006; Kuwahara, 2006).

The Crystal Size Distributions (CSDs) of illite and illite-smectite samples were studied by Eberl *et al*. (1998) and Środoń *et al*. (2000) using TEM imaging. The CSDs may have distinctive shapes related to the mineral's crystal-growth history: nucleation, growth in an open or closed system, Ostwald ripening, *etc*. The CSDs method was used by Christidis (2001) to study a bentonite from Greece. Only the length and width of particles were measured, suggesting supply-controlled crystal growth in an open system or random ripening in a closed system.

An alternate approach to studying clay morphology is high-resolution, low-pressure argon adsorption, a method based on surface-energy heterogeneity analysis, using the summation of the local derivative isotherms method (Villiéras *et al*., 1992, 1997a, 1997b, 2002; Michot and Villiéras, 2006). The validity of this method was first tested on kaolinite and sepiolite *via* comparison of results obtained with those from low-temperature adsorption microcalorimetry (Villiéras *et al*., 1992, 1997a). More recently, the study of the geometric properties of smectite, kaolinite, and illite using both AFM and argon adsorption (Tournassat *et al.*, 2003, Sayed Hassan *et al*., 2006) demonstrated the consistency

* E-mail address of corresponding author:
sabine.petit@univ-poitiers.fr
DOI: 10.1346/CCMN.2014.0620203

https://doi.org/10.1346/CCMN.2014.0620203 Published online by Cambridge University Press

Table 1. Coherent scattering domain size (CSDS) of nontronite particles from powder XRD data.

T (ºC)	(001)		(06,33)
	H (Å)	*N*	D (Å)
150	76	6.3	189
125	63	5.2	190
110	50	4.1	138
100	45	3.8	142
90	48	4.0	114
75	nm	nm	nm

H = crystal coherency along the c* direction (air dry conditions, Na as interlayer cation); *N* = number of stacked layers (assuming d_{001} = 12 Å); *D* = crystal coherency in the (001) layer plane; nm = not measurable (crystallinity too low).

between these two methods. Argon adsorption has also been used to study the shape and size of smectite particles, including saponite (Michot and Villiéras, 2002), montmorillonite, and nontronite (Tournassat *et al.*, 2003; Peronnet *et al.*, 2007; Le Forestier *et al.*, 2010). High-resolution, low-pressure argon adsorption enables the simultaneous investigation of all of the clay particles in a sample, which results in the accurate determination of mean basal and edge surface areas (Sayed Hassan *et al.*, 2006).

The objective of this study was to determine changes in particle shape and size in a series of nontronite samples as a function of synthesis temperature, by applying high-resolution, low-pressure argon adsorption.

MATERIALS AND METHODS

Sample description and characterization

A series of nontronite samples was synthesized by Decarreau *et al.* (2008) from a coprecipitated gel with the composition $Si_2FeNa_2O_6.nH_2O$ over a 4-week period at temperatures that ranged from 75 to 150ºC. Nontronite was demonstrated to be the only mineral that could precipitate under these synthesis conditions (Decarreau *et al.*, 2004, 2008). These synthetic nontronites were studied in detail using X-ray diffraction (XRD), TEM, chemical analyses, differential thermal and gravimetric analysis (DTA-DTG), and Fourier-transform infrared (FTIR), Mössbauer, and X-ray absorption near edge (XANES) spectroscopies (Decarreau *et al.*, 2008). Irrespective of the synthesis temperature, the nontronite samples exhibited the same structural formula of $(Si_{3.25}Fe^{3+}_{0.75})Fe^{3+}_2O_{10}(OH)_2,Na_{0.75}$. An increase in the synthesis temperature increased the crystallinity of samples. The synthesis products consisted of nontronite and some amorphous residual phase. As determined from the DTG data (Decarreau *et al.*, 2008), the proportion of starting gel which crystallized into nontronite increased from 70% to >90% with the increase in synthesis temperature. Taking into account the uncertainties in the DTG data, the samples obtained at 125 and 150ºC were assumed to be of pure nontronite.

From XRD powder data (Decarreau *et al.*, 2008), the coherent scattering domain size (CSDS) (Moore and Reynolds, 1989, p. 87) was measured using the Scherrer equation ($L = K{\cdot}\lambda/B{\cdot}\cos\theta$) in the (001) plane and along the [001]* direction (also known as the c* direction) from the widths of the (06,33) and (001) reflections, respectively (Table 1). The K values in the Scherrer equation were 1 for the (001) reflection and 1.91 for the (06,33) composite reflection (Brindley and Brown, 1980, pp. 131, 139). When the synthesis temperature was increased, the CSDS in the plane of the layers was increased at temperatures from 75 to 125ºC, and then remained constant (Figure 1). Along the c* direction, the CSDS remained constant between 75 and 100ºC and then increased slightly (Figure 1). Using a d_{001} value of 12 Å, the number of stacked layers as determined from the XRD data was between 4 and 6.

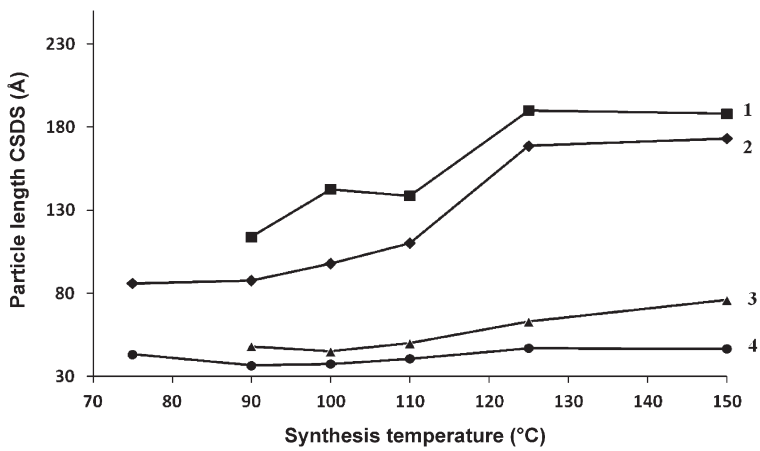


Figure 1. Coherent scattering domain size (CSDS) (from XRD, in the layer plane (2) and in the c* direction (3)) and dimensions (from argon adsorption: particle length (1) and thickness (4)) of particles *vs.* synthesis temperature of nontronites.

https://doi.org/10.1346/CCMN.2014.0620203 Published online by Cambridge University Press

In the TEM images (Decarreau *et al.*, 2008), irrespective of the synthesis temperature, isolated nontronite particles appeared as crumpled flakes with rolled edges associated in micron-sized aggregates. The TEM images showed that the aggregates contained numerous particles <10 nm in size. These small particles were less evident in the samples prepared at 125 and 150ºC. The largest observed particles were 400 nm for the sample prepared at 150ºC. Even after strong ultrasonic treatment, the nontronite particles still formed thick aggregates irrespective of the sample: a measurement of the particle-size distribution was not possible.

Low-pressure argon adsorption at 77 K

The fundamentals of the low-pressure argon adsorption approach and the derivative isotherm summation (DIS) method were given by Villiéras *et al.* (1992, 1997a, 1997b, 2002). The low-pressure isotherms of argon adsorption at 77 K were recorded using a lab-built, automatic, quasi-equilibrium volumetric apparatus (Michot *et al.*, 1990; Villiéras *et al.*, 1992, 1997b). Approximately 1 g of the sample was outgassed overnight at 110ºC under a residual pressure of 10^{-4} Pa. After the samples were outgassed, a slow and constant flow of argon was introduced into the adsorption cell through a micro-leak up to the Brunauer-Emmet-Teller (BET) domain ($P/P_0 \geqslant 0.15$). If the flow rate is sufficiently low, the measured pressures are considered to be quasi-equilibrium pressures (in the range of 10^{-3} to 3×10^4 Pa). From the recording of the quasi-equilibrium pressure as a function of time, high-resolution adsorption isotherms were obtained for the apparent filling of the first monolayer (± BET Monolayer capacity, $0.08 \geqslant P/P_0 \geqslant 0.15$) with >2000 experimental data points. The derivative of the adsorbed quantity is calculated as a function of the logarithm of the relative pressure, $\ln(P/P_0)$, which corresponds to the free energy of adsorption in kT or RT units (Villiéras *et al.*, 1992, 1997a). The total derivative adsorption isotherm on a heterogeneous surface is then simulated by the sum of the local theoretical derivative adsorption isotherms using concepts that describe the adsorption phenomena on heterogeneous surfaces and the DIS procedure (Villiéras *et al.*, 1992, 1997a). For each local isotherm, the BET multilayer adsorption model was used and the following parameters obtained: ω, the lateral interaction between two neighboring adsorbed molecules; $\ln(P/P_0)$, the position of the peak; and *V*m, the monolayer capacity. The DIS fitting procedure has been described extensively by Villiéras *et al.* (1992, 1997a, 1997b, 2002) and, for swelling clays, by Perronnet *et al.* (2007).

For clay minerals with large cations (*e.g.* K^+) on their external surfaces, the values of the basal surface and edge surface areas measured by low-pressure argon adsorption can be significantly smaller as shown by Sayed-Hassan *et al.* (2005) for kaolinite edge surfaces and by Bardot *et al.* (1998) for illite basal and edge surfaces. Therefore, prior to the adsorption experiments, the clay samples were Na^+-saturated using a 1 M NaCl solution and washed until all excess ions were removed, as indicated by the $AgNO_3$ test.

RESULTS

Irrespective of the synthesis temperature, the derivative isotherms of the low-pressure argon adsorption of the synthesized nontronites exhibited the same features (Figure 2). As typical for phyllosilicates (Sayed Hassan *et al.*, 2006; Villiéras *et al.*, 1992, 1997a, 1997b), the derivative isotherms exhibited a peak at $\ln(P/P_0)$ near −4 to −5, and a shoulder and a tail at greater energy (*i.e.* at lower values of $\ln(P/P_0)$). For kaolinite, the main peak at low energy could be assigned to the adsorption on basal faces while the shoulder at higher energy and high-energy adsorption peaks could be assigned to the adsorption on edge faces (Villiéras *et al.*, 1992). Further studies demonstrated that the DIS peak attribution for kaolinite could be applied to argon adsorption on other clay minerals including smectites (*e.g.* Villiéras *et al.*, 1992; Perronnet *et al.*, 2007; Sayed Hassan *et al.*, 2006).

Each derivative adsorption isotherm could be fitted using the DIS procedure (Villiéras *et al.*, 1997a; Bardot *et al.*, 1998; Sayed Hassan *et al.*, 2005, 2006; Perronnet *et al.*, 2007) with five characteristic adsorption domains (Figure 3, Table 2). The parameters of the DIS procedure were similar for the samples that were synthesized at 125 and 150ºC (Table 2). In the present case, the total derivative isotherms for clay minerals could be modeled using three BET local-derivative isotherms at greater energies (domains 3−5 in Table 2) which were attributed to the adsorption on the edge surfaces, and two local derivative isotherms at lower energies (domains 1 and 2 in Table 2) which were attributed to adsorption on the basal surfaces.

The derivative curve of the starting gel (Figure 2) differed substantially from those of the nontronites synthesized. Most notably, the derivative curve of the starting gel did not exhibit a clear peak at $\ln(P/P_0)$ at approximately −4 to −5, *i.e.* characteristic of poorly crystallized solids, such as amorphous silica (Villiéras *et al.*, 1998; Rudzinski *et al.*, 1999). Observations by TEM of similar gels revealed that they contain rounded particles, with diameters of ~200 Å, organized as diffuse aggregates (Decarreau *et al.*, 1987). The measured total surface area (*TSA*) of the gel was 127 m^2/g (Table 3), a value corresponding to spherical particles with a diameter of 160 Å, in reasonable agreement with the TEM results. Thus, the edge surface area (*ESA*) and basal surface area (*BSA*) estimates from argon adsorption were irrelevant for the starting gel (Table 3).

For all of the other samples, the peak positions at $\ln(P/P_0) \approx -5$ and at $\ln(P/P_0) \approx -7$ were typical of basal and edge surfaces with Na^+ as surface-exchange-

https://doi.org/10.1346/CCMN.2014.0620203 Published online by Cambridge University Press

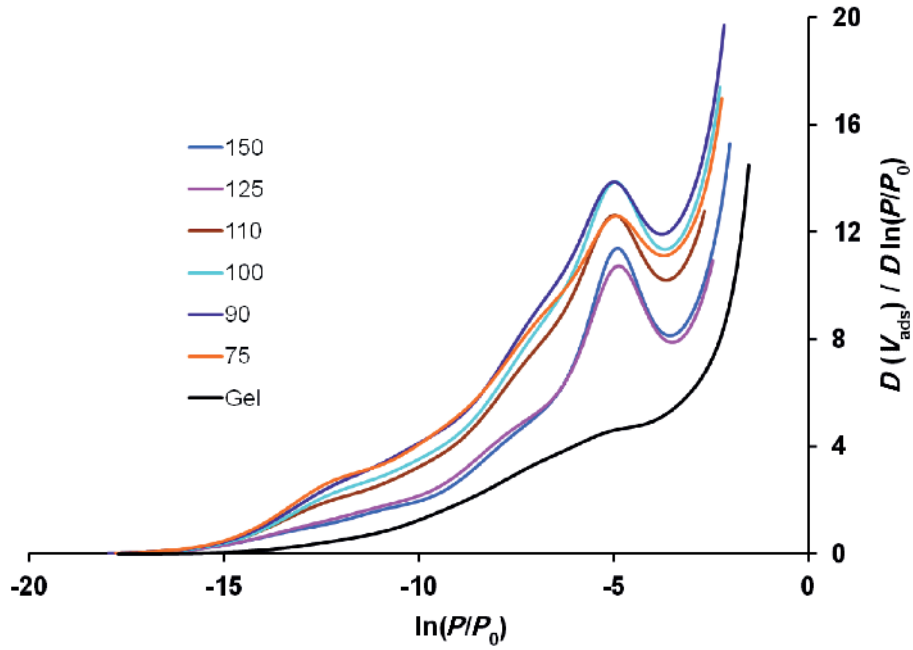


Figure 2. Derivative isotherms of low-pressure argon adsorption at 77 K of synthetic nontronites. The numbers on the key refer to the synthesis temperature (ºC). Gel: starting gel.

able cations (Bardot *et al.*, 1998), as expected given the sample-preparation procedure. The evolution of the lateral interaction parameter ω/kt for domain 2, which ranged from 0.5 for the starting gel to 1.4 for the 150ºC sample, indicated clearly that the surface homogeneity for argon increased with increasing synthesis temperature. Following Villiéras *et al*. (1997b) and Perronnet *et al.* (2007), the number of surface defects or the surface roughness on the basal surfaces of the nontronite samples were assumed to decrease, therefore.

The *BSA*, *ESA*, and *TSA* were calculated on the basis of a 13.8 Å^2 cross-sectional area for adsorbed argon (Table 3).

Nontronite particles were treated as circular disks to estimate the mean dimensions. The thickness (*H*) and particle length (*D*) of the particles (Table 3) were calculated from the *BSA* and *ESA* using the equations:

$$H = 2/BSA \cdot \rho \text{ and } D = 4/ESA \cdot \rho \quad (1)$$

where ρ is the particle density (3.0 g/cm^3 according to the structural formula). Several clear trends appeared

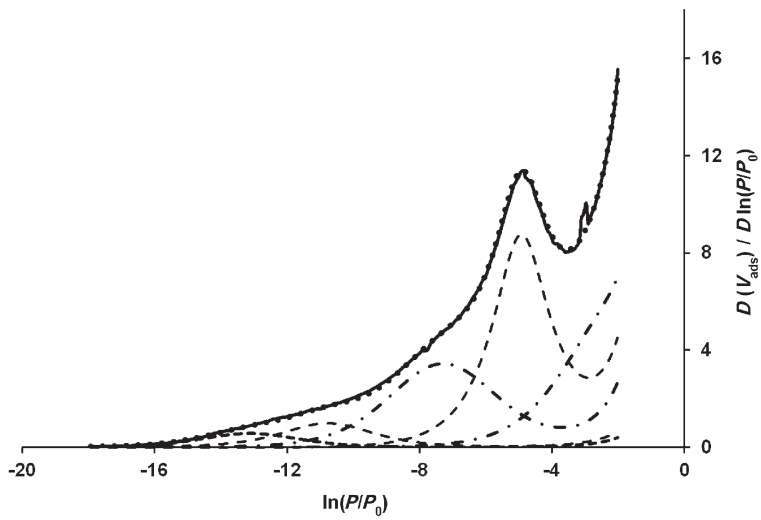


Figure 3. Experimental derivative argon adsorption obtained at 77 K for the nontronite synthesized at 150ºC and its decomposition using the derivative isotherm summation (DIS) method. Solid line: experimental; dotted line: fit; dashed lines: adsorption domains obtained using the DIS procedure.

https://doi.org/10.1346/CCMN.2014.0620203 Published online by Cambridge University Press

Table 2. Main parameters obtained from the application of the DIS method to argon adsorption at 77 K on synthesized nontronites.

	DIS domain parameters	Synthesis temperature (ºC)						
		Starting gel	75	90	100	110	125	150
Domain 1	$\ln(P/P_0)$	−2.61	−2.70	−2.61	−2.58	−2.55	−2.40	−2.46
	Vm (cm^3/g)	13.6	21.8	25.1	23.4	19.9	15.0	16.7
	ω/*KT*	0	0	0	0	0	0	0
Domain 2	$\ln(P/P_0)$	−5.04	−4.95	−5.01	−4.98	−4.98	−4.89	−4.92
	Vm (cm^3/g)	7.9	19.6	23.8	24.5	24.4	23.1	22.1
	ω/*KT*	0.5	1.1	1.1	1.2	1.1	1.2	1.4
Domain 3	$\ln(P/P_0)$	−6.93	−6.84	−6.93	−6.93	−7.05	−7.44	−7.29
	Vm (cm^3/g)	8.2	23.9	24.7	22.6	20.1	14.8	14.8
	ω/*KT*	0	0	0	0	0	−0.2	−0.3
Domain 4	$\ln(P/P_0)$	−9.21	−9.48	−9.84	−9.78	−9.87	−10.77	−10.77
	Vm (cm^3/g)	3.4	9.9	9.7	7.8	7.1	4.3	3.7
	ω/*KT*	0	0	0	0	0	0	0.2
Domain 5	$\ln(P/P_0)$	−11.91	−12.21	−12.27	−12.24	−12.42	−13.02	−13.14
	Vm (cm^3/g)	1.1	8.1	6.6	6.2	5.3	2.3	2.2
	ω/*KT*	0	0	0	0	0	0	0

$\ln(P/P_0)$: peak position in logarithm of the relative argon pressure unit; Vm (cm^3/g): monolayer capacity; ω/*KT*: lateral interaction between two neighboring adsorbed molecules.

from these data. The synthesis temperature affected the size and shape of the nontronite particles (Table 3). The *TSA* decreased from 75 to 125ºC and remained fixed between 125 and 150ºC (Figure 4). The decrease in the *TSA* was not related to the last appearance of the gel when the synthesis temperature was increased. In fact, the last appearance of the gel would be expected to promote an increase in the *TSA*. The observed decrease in the *TSA* was related to an increase in the particle size of the smectites synthesized (Decarreau, 1980; Decarreau and Bonnin, 1986; Decarreau *et al.*, 1987). In contrast, the *ESA* and *BSA* (expressed as % of the *TSA*) exhibited opposite trends (Figure 5): between 75 and 125ºC the *BSA* increased whereas the *ESA* decreased, and the *ESA* and *BSA* did not change between 125 and 150ºC. These trends are related to an increase in the particle length, although the thickness did not change significantly (Figure 1). The mean diameter of the synthetic nontronites increased from 86 to 173 Å between 75 and 125ºC and did not increase between 125 and 150ºC. For all of the synthesis temperatures, the mean thickness of the particles remained nearly constant at 40 Å. The d_{001} value was 10 Å under the argon-adsorption experimental conditions. Under these conditions, the mean number of stacked layers for the synthesized nontronites was four, irrespective of the synthesis temperature.

For the nontronite samples that were synthesized at 75 and 100ºC, the maximum amount of remaining gel was 30% (Decarreau *et al.*, 2008). Although the *TSA* of the gel was low, the *TSA* of the nontronite particles was slightly larger because the *TSA* was measured for the entire sample. The derivative adsorption isotherm of the starting gel was fitted by the DIS method using the five absorption domains similar to those of nontronite, in

Table 3. Basal surface area (*BSA*), edge surface area (*ESA*), total surface area (*TSA*) (m^2/g), thickness (*H*), and particle length (*D*) of synthesized nontronite particles obtained from low-pressure argon adsorption data. Values given in italics are *BSA* and *ESA* expressed as a percentage of *TSA*.

Synthesis temperature (ºC)	Starting gel	75	90	100	110	125	150
BSA		154 *50*	182 *53*	178 *56*	164 *57*	142 *64*	143 *65*
ESA		155 *50*	152 *47*	136 *44*	121 *43*	79 *36*	77 *35*
TSA	127	309	333	313	285	221	220
H		43	37	37	41	47	47
D		86	88	98	110	169	173

https://doi.org/10.1346/CCMN.2014.0620203 Published online by Cambridge University Press

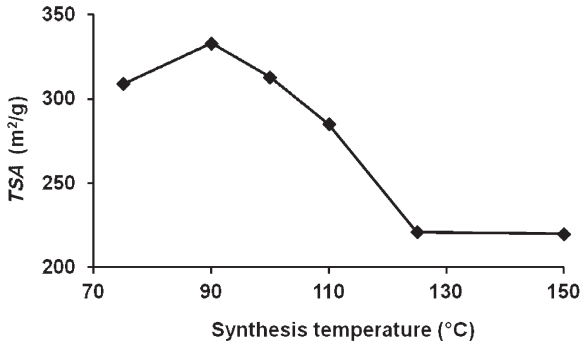


Figure 4. Total surface area (*TSA*) (m^2/g) of nontronite particles (from argon adsorption) *vs.* synthesis temperature.

order to evaluate the gel contribution in argon adsorption on the whole sample (Table 2). The measured *TSA* for each sample was then equal to the sum of the nontronite *TSA* and starting-gel *TSA*. The actual values of the *TSA*, *ESA*, and *BSA* of nontronite could be obtained, using the gel:nontronite weight ratio determined from DTG data and using the data in Table 2, for the five adsorption domains. Using a mixing model, the *TSA* of nontronite would increase but the *ESA*/*BSA* ratio would not change (not shown). This mixing model could not be applied quantitatively because the gel:nontronite weight ratio, as measured by DTG, was not sufficiently precise, and the *TSA* of the remaining untransformed product might have been different from that of the starting gel and might differ from one sample to another.

DISCUSSION

Consistency of data

The XRD data and the argon adsorption data followed the same trend. The parameters measured were in the same range but were not equal (Tables 1, 3; Figure 1).

Both data sets showed an increase in the particle length and CSDS in the (001) plane of nontronite particles synthesized at temperatures from 75 to 125ºC, and these values remained constant for samples prepared at 150ºC. The CSDS that were measured by XRD are slightly greater than the mean particle lengths that were measured by argon adsorption. The XRD data gave the mean length of the crystallographic lattice without any defects (single crystal). The CSDS, in the (001) plane, as measured by XRD, cannot be greater than the particle length of nontronite. The differences between the XRD and argon adsorption data are probably explained by the uncertainties in the measurements.

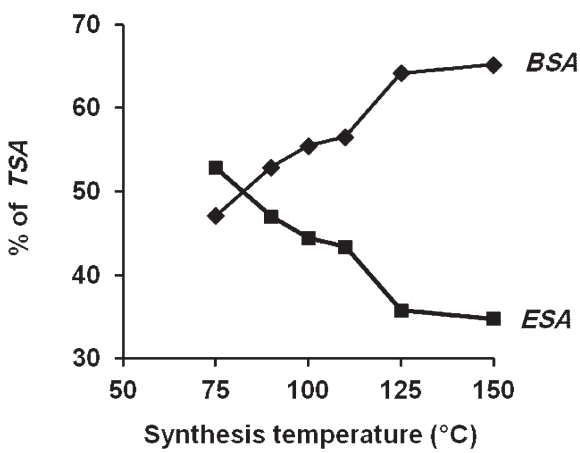


Figure 5. Relative (% of total surface area, *TSA*) ratio of edge surface area (*ESA*) and basal surface area (*BSA*) of nontronite particles (from argon adsorption) *vs.* synthesis temperature.

According to both data sets, the mean number of stacked layers (*N*) in nontronite was four for samples synthesized at temperatures from 75 to 110ºC. For samples prepared at 125 to 150ºC, *N* increased slightly (by <1 layer) according to the argon data and was six according to the powder XRD data. The number of stacked layers, as measured by argon adsorption, was apparently four for all samples. The discrepancy between the XRD and argon adsorption data may be related to inter-particle diffraction (Eberl *et al.*, 1998) for nontronites prepared at higher temperatures. Argon adsorption appears to reflect the actual size and shape of the nontronite particles better than the values obtained from the XRD data.

Crystal growth of smectites

Synthesized nontronite crystal growth. Because nontronite is the only mineral phase that can precipitate under the experimental conditions used (Decarreau *et al.*, 2008; Andrieux and Petit, 2010), the chemical evolution of the system involves only the nucleation and growth of nontronite. The influences of the synthesis duration and temperature on similar nontronite crystallization were studied by Decarreau (1980) and Decarreau *et al.* (1987). The smectite crystal size within the (001) plane was time dependent, and the kinetics of crystal growth followed the Arrhenius equation (Carrado *et al.*, 2006). The mean particle length (*D*), within the (001) plane was:

$$D = A \cdot \exp(-E/RT) \cdot t$$

where *t* is time and *T* is absolute temperature. For the present experiments, time and temperature played analogous roles. Syntheses performed at increased temperatures with a fixed aging time were analogous to syntheses performed at a fixed temperature with increased aging times. In the present work, as the synthesis temperature increased, the number of stacked layers did not increase significantly, although the mean length of the particles doubled. This observation suggests that the crystal growth was dominated by the lateral extension of the synthesized nontronite layers. This lateral extension measured for the synthetic nontronites is a crystal-growth process that differs from those usually described for clay minerals that are more three-dimensional, such as kaolinite, chlorite, and mica. Polygonal and/or broadly circular spiral-growth

https://doi.org/10.1346/CCMN.2014.0620203 Published online by Cambridge University Press

patterns have often been observed on the growth surfaces of biotite (Amelinks, 1952), phlogopite (Baronnet, 1972), illite (Inoue and Kitagawa, 1994; Kitagawa, 1998), rectorite (Kitagawa, 1997), kaolinite (Sunagawa and Koshino, 1975), and mixed-layer illite-smectite (Kitagawa and Matsuda, 1992). Two-dimensional nucleation was observed on the (001) growth surfaces of sudoite (Jige *et al.*, 2003), which produced an increase in the number of stacked layers. The latter crystal-growth process is less commonly observed because a greater degree of fluid oversaturation is required.

Using the periodic bond chain (PBC) theory of Hartman (1973), a large number of defects in clay minerals was suggested by Meunier (2010) to disrupt the PBCs, thus precluding crystal growth. The PBCs present in this study were those within the (001) plane, *i.e.* the PBCs of [100], [110], and [$\bar{1}$10]. Following Meunier (2010), the PBC theory of Hartman (1973) suggests implicitly a crystal-growth process of clay minerals essentially bi-dimensional within the (001) plane, which was observed for the synthetic nontronites here.

During crystal growth, an increase in the particle size entailed a decrease in the *TSA* per unit mass. For a constant number of stacked layers in the clay particles, the *BSA* per unit mass is constant during crystal growth (H = constant in relation 1), and a decrease in the *TSA* is only due to a decrease in the *ESA*. This relation was observed for the synthesized nontronites (Table 3): the *BSA* fluctuated around a mean value of 160 m^2/g, whereas the *ESA* decreased continuously from 115 to 77 m^2/g. The theoretical values of the *TSA* for circular particles, having a constant 40 Å thickness, were calculated as a function of the particle diameter (Figure 6). The measured *TSA* of the synthetic nontronites, obtained by the DIS procedure from the argon adsorption curves, fitted the theoretical curve well (Figure 6).

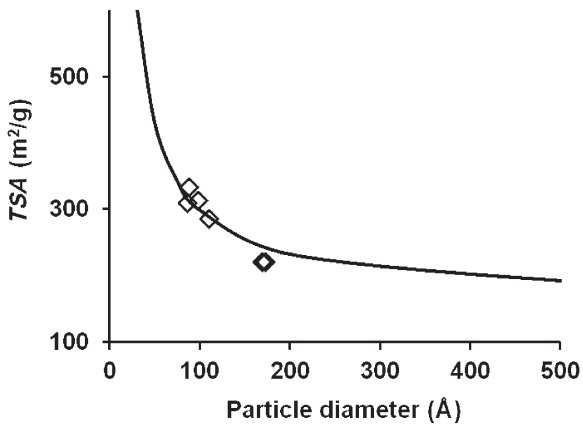


Figure 6. Total surface area (*TSA*) (m^2/g) of nontronite particles *vs.* their mean particle length. Solid line: theoretical *TSA* calculated for circular particles with a constant thickness of 40 Å. Open diamonds: *TSA* values measured from argon adsorption.

The work above demonstrated that the crystal growth of the synthetic nontronites occurred *via* the addition of material ('building blocks') to the edges of particles, mainly. These 'building blocks' were probably less than four layers thick but their structure could not be determined in detail. Consequently, the stacked layers might not have the same planar extension, inducing local strength. This crystal growth may explain the rolled edges of the particles as observed by TEM (Decarreau *et al*., 2008).

The crystal growth of the nontronites was similar for samples prepared at 125 and 150ºC. Because nontronite becomes unstable and aegirine occurs at higher temperatures (Decarreau *et al.* 2004), long synthesis times (*i.e.* several years, Decarreau *et al.*, 1987) would be required to obtain larger crystals experimentally.

Effect of particle size on OH-stretching vibrations. The ν OH bandwidth in infrared spectra is partially linked to the size of particles due to the "crystallinity" effect (Petit *et al*., 2004, 2008). A decrease in the ν Fe_2^{3+}-OH band width in IR spectra of synthetic nontronites was noted by Decarreau *et al.* (2008) when the synthesis temperature increased. The plot of the ν Fe_2^{3+}-OH band width *vs.* the mean particle length, obtained from argon adsorption, revealed that the band width reached a plateau at 45 cm^{-1} from a particle length of ~180 Å (Figure 7).

Comparison with other synthetic smectites. The crystal growth of plate-shaped smectite *via* the lateral extension of layers is in agreement with the data from Decarreau (1980) and Decarreau *et al.* (1987). In these previous studies, the CSDS of synthetic Mg-smectite (stevensite) and of various synthetic nontronites were measured. The authors observed a small increase in the number of stacked layers (from two to six) and an increase along the (001) plane with an increase in the synthesis time or temperature.

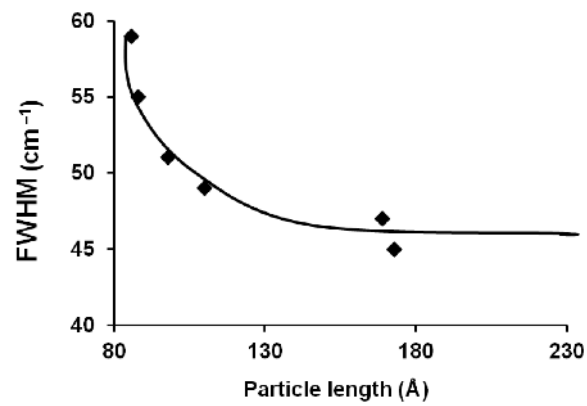


Figure 7. Full width at half maximum (FWHM) of the ν Fe_2^{3+}-OH band observed on the MIR spectra of synthetic nontronites *vs.* the mean length of the particles.

https://doi.org/10.1346/CCMN.2014.0620203 Published online by Cambridge University Press

Synthetic saponite (Michot and Villiéras, 2002) and montmorillonite (Le Forestier *et al.*, 2010) were also studied using low-pressure argon adsorption. Syntheses were performed for four weeks at 400ºC at 1 kbar (various charges) for the saponite series and at 350ºC and 1.2 kbar for montmorillonite. The derivative adsorption curves were similar to those of the synthetic nontronite presented here. The saponite particles were 200−600 nm wide (mean of 315 nm) and 17−39 nm thick (mean of 25 nm). These synthetic saponite crystals were ~20 times greater in the lateral dimension and only six times thicker than the largest nontronites synthesized here. The montmorillonite synthesized was 65 nm in-plane and 12 nm thick. Unfortunately, these synthetic saponite samples and montmorillonite were obtained for only one aging time and only one temperature; consequently, the crystal-growth process could not be deduced. Nevertheless, even for synthesis temperatures >300ºC, synthetic smectites contained 12−39 stacked layers which resulted in a thickness much smaller than the plane extension.

Despite the high synthesis temperature, the montmorillonite particles were only three to four times larger than the nontronite particles studied, and had a similar *H*/*D* ratio. For dioctahedral smectites (*e.g.* montmorillonite and nontronite) a moderate increase in synthesis temperature (or time) did not result in a significant increase in the particles size. In contrast, large smectite crystals were synthesized under extreme conditions by Nakasawa *et al.* (1992).

Trioctahedral smectite particles were shown by Decarreau (1980, 1983) and Decarreau *et al.* (1987) to be generally larger than dioctahedral smectite particles in samples prepared under similar synthesis conditions. Accordingly, argon adsorption measurements revealed that saponite particles were significantly larger (ten times) than the montmorillonite particles that were synthesized under similar conditions (Michot and Villiéras, 2002; Le Forestier *et al.*, 2010).

Syntheses performed in the temperature range of weathering or hydrothermal systems indicated that the small size of dioctahedral smectites was constrained by the crystal-growth processes.

Comparison with natural smectites. The particle morphologies of various natural smectites have been studied using low-pressure argon adsorption, including those of MX80 montmorillonite (Tournassat *et al.*, 2003), two montmorillonites and one nontronite (Fe^{3+}-rich beidellite) (Perronnet *et al.*, 2007), and SWy2 montmorillonite samples (Le Forestier *et al.*, 2010). These smectites were derived from bentonites, which resulted from the interaction of volcanic ash falls and ocean water (Moll, 2001; Christidis and Huff, 2009). From the oxygen and hydrogen isotopic data (Arslan *et al.*, 2010 and references therein), bentonites were determined to form at relatively low temperatures (<100ºC). The particles of these natural smectites have a size range similar to those of synthetic dioctahedral smectites, though the MX80 and SWy2 smectites contained additional stacked layers (28 nm and 34 nm thick, respectively) compared to synthetic smectites (11−15 nm thick) according to Perronnet *et al.* (2007).

The data that were obtained for natural bentonites are in agreement with the data from experimental systems (Meunier, 2006), suggesting similar crystal-growth processes.

Clay minerals that form at the Earth's surface and under sub-surface conditions exhibit a small particle size, whereas the associated minerals are generally not as small. The PBC theory (Hartman, 1973) was suggested by Meunier (2006) to be applicable to clay minerals, thus precluding their crystal growth. Implicitly, the crystal growth of clay minerals is essentially two-dimensional (Meunier, 2006) (see above) as demonstrated here both for natural and synthetic smectites.

Smectite crystal-growth mechanisms. As far as the authors are aware, no data on the crystal-growth mechanisms of smectites are available in the literature. The only permanent portion of the smectite structure is the layer because the interlayer can vary in both size and chemistry, depending on the chemistry of the surrounding fluid. Consequently, crystal-growth mechanisms in three dimensions (*e.g.* polygonal and spiral-growth patterns) are unlikely to occur for smectite. The crystal-growth pattern that was determined for synthetic nontronite, *i.e.* the lateral growth of the layer only, probably occurs for synthetic and natural dioctahedral smectites. This conclusion is suggested by the similarity of the morphologies of natural and synthetic dioctahedral smectite. For synthetic nontronite, the number of stacked layers (*i.e.* four) can crystallize during the nucleation stage of crystal growth or slightly afterward; smectites that were synthesized over a few days at 25ºC exhibited a broad 001 XRD reflection due to three or four stacked layers (Decarreau, 1980, 1983; Decarreau and Bonnin, 1986; Decarreau *et al.*, 1987). For natural smectite and smectites that were synthesized at higher temperatures, particles with 10 to 40 stacked layers may represent another crystal-growth process. The AFM images of the MX 80 sample (Tournassat *et al.*, 2003) showed broadly circular "islands" on the (001) surfaces of isolated particles 10−200 nm wide. These islands were one layer thick. This feature was consistent with the close-step pattern of two-dimensional growth, which led to an increase in the number of stacked layers. Such a growth pattern was observed for metamorphic mica (Sunagawa and Koshino, 1975) and hydrothermal sudoite (Jige *et al.*, 2003). However, only two-dimensional crystal-growth processes occur during smectite formation. The remaining questions are as follows: what is the crystal-growth unit (building block) and does this

https://doi.org/10.1346/CCMN.2014.0620203 Published online by Cambridge University Press

unit include an interlayer cation? For epitaxial growth of trioctahedral clay, nucleation began *via* the formation of a hydroxide sheet on which silica was adsorbed (Manceau *et al.*, 1999; Rainer *et al.*, 2002; Schegel *et al.*, 2001). This model, proposed by Caillère *et al.* (1956, 1957) and often used since, was based on the similarity of structures of trioctahedral Mg, Ni, and Co hydroxides and the analogous octahedral sheet of trioctahedral clay minerals. The process was different for dioctahedral structures (Decarreau, 1983). The building blocks were demonstrated to be [Si tetrahedra-Al (or Fe) octahedra-Si tetrahedra] 'monomers' for TOT dioctahedral clays (Siffert, 1962). These monomers might be the smaller building block for the crystal growth of dioctahedral TOT clays (White and Zelazny, 1988).

ACKNOWLEDGMENTS

The authors thank an anonymous reviewer, Douglas McCarty, and Utpalendu Kuila for their constructive comments that helped to improve the manuscript.

REFERENCES

Amelinckx, S. (1952) La croissance hélicoïdale de cristaux de biotite. *Comptes Rendus de l'Académie des Sciences, Paris*, **234**, 971–973.

Andrieux, P. and Petit, S. (2010) Hydrothermal synthesis of dioctahedral smectites: The Al-Fe chemical series. Part I: Influence of experimental conditions. *Applied Clay Science*, **48**, 5–17.

Arslan, M., Abdioglu, E., and Kadir, S. (2010) Mineralogy, geochemistry and origin of bentonite in upper cretaceous pyroclastic units of the Tirebolu area, Giresun, northeast Turkey. *Clays and Clay Minerals*, **58**, 120–141.

Bauer, A., Lanson, B., Ferrage, E., Emmerick, K., Taubald, H., Schield, D., and Velde, B. (2006) The fate of smectite in KOH solution. *American Mineralogist*, **91**, 1313–1322.

Bardot, F., Villiéras, F., Michot, L.J., François, M., Gérard, G., and Cases, J.M. (1998) High resolution gas adsorption study on illites permuted with various cations: assessment of surface energetic properties. *Journal of Dispersion Science and Technology*, **19**, 739–759.

Baronnet, A. (1972) Growth mechanisms and polytypism in synthetic hydroxyl bearing phlogopite. *American Mineralogist*, **47**, 605–616.

Bickmore, B.R., Bosbach, D., Hochella, M.F., Charlet, L., and Rufe, F. (2001) In situ atomic force microscopy study of hectorite and nontronite dissolution: Implications for phyllosilicates edge surface structures and dissolution mechanisms. *American Mineralogist*, **86**, 411–423.

Brindley, G.W. and Brown, G. editors (1980) *Crystal Structure of Clay Minerals and their X-ray Identification.* Monograph **5**, Mineralogical Society, London.

Caillère, S., Henin, S., and Esquevin, J. (1956) Etude expérimentale du mécanisme de la formation des antigorites nickellifères. *Bulletin de la Société Française de Minéralogie Cristallographie*, **79**, 408–421.

Caillère, S., Henin, S., and Esquevin, J. (1957) Synthèse des minéraux argileux. *Bulletin du Groupe Français des Argiles*, **9**, 67–76.

Carrado, K., Decarreau, A., Petit, S., Bergaya, F., and Lagaly, G. (2006) Synthetic clay minerals and purification of natural clays. Pp. 115–139 in: *Handbook of Clay Science* (F. Bergaya, B.K.G. Theng, and G. Lagaly, editors). Elsevier, Amsterdam.

Christidis, G.E. (2001) Formation and growth of smectites in bentonites: a case study from Kimols Island, Aegean, Greece. *Clays and Clay Minerals*, **49**, 204–215.

Christidis, G.E. and Huff, W.D. (2009) Geological aspects and genesis of bentonites. *Elements*, **5**, 93–98.

Decarreau, A. (1980) Cristallogenèse expérimentale des smectites magnésiennes: hectorites, stévensites. *Bulletin de Minéralogie*, **103**, 579–590.

Decarreau, A. (1983) Etude expérimentale de la cristallogenèse des smectites. Mesure des coefficients de partage smectite trioctaèdrique – solution aqueuse pour les métaux M^{2+} de la première série de transition. *Sciences Géologiques*, Mémoire n°**74**, 185 pp.

Decarreau, A. and Bonnin, D. (1986) Synthesis and crystallogenesis at low temperature of Fe(III)-smectites by evolution of coprecipitated gels: experiments in partially reducing conditions. *Clay Minerals*, **21**, 861–877.

Decarreau, A., Bonnin, D., Badaut-Trauth, D., Couty, R., and Kaiser, P. (1987) Synthesis and crysytallogenesis of ferric smectite by evolution of Si-Fe coprecipitation in oxidizing conditions. *Clay Minerals*, **22**, 207–223.

Decarreau, A., Petit, S., Vieillard, Ph., and Dabert, N. (2004) Hydrothermal synthesis of aegirine at 200ºC. *European Journal of Mineralogy*, **16**, 85–90.

Decarreau, A., Petit, S., Martin, F., Farges, F., Vieillard, Ph., and Joussein, E. (2008) Hydrothermal synthesis, between 75 and 150ºC, of high charge ferric nontronites. *Clays and Clay Minerals*, **56**, 322– 337.

Eberl, D.D., Drits V.A., and Środoń, J. (1998) Deducing growth mechanism for minerals from the shapes of crystal size distributions. *American Journal of Science*, **298**, 499–533.

Güven, N. (1988) Smectites. Pp. 497–559 in: *Hydrous Phyllosilicates (exclusive of Micas)* (S.W. Bailey, editor). Reviews in Mineralogy, **19**, Mineralogical Society of America, Washington DC.

Hartman, P. (1973) Structure and morphology. Pp. 367–402 in: *Crystal Growth: an Introduction* (P. Hartman, editor). North Holland Publications, Amsterdam.

Inoue, A. and Kitagawa, R. (1994) Morphological characteristics of illitic clay minerals from a hydrothermal system. *American Mineralogist*, **79**, 700–711.

Jige, M., Kitagawa, R., Zaykov, V.V. and Sinyakovskaya, I. (2003) Surface microtopography of sudoite. *Clay Minerals* **38**, 375–382.

Kitagawa, R. (1997) Surface microtopography of rectorite (allevardite) from Allevard, France. *Clay Minerals*, **29**, 709–715.

Kitagawa, R. (1998) Surface microtopography of illite crystals from different modes of occurrence. *The Canadian Mineralogist*, **36**, 1559–1567.

Kitagawa, R. and Matsuda, T. (1992) Microtopography of regularly interstratified mica and smectite. *Clays and Clay Minerals*, **40**, 114–121.

Kloprogge, J.T., Komarneni, S., and Amonette, J.E. (1999) Synthesis of smectite clay minerals: a critical review. *Clays and Clay Minerals*, **47**, 529–554.

Kuwahara, Y. (2006) In-situ AFM study of smectite dissolution under alkaline conditions at room temperature. *American Mineralogist*, **91**, 1142–1149.

Le Forestier, L., Muller, F., Villiéras, F., and Pelletier, M. (2010) Textural and hydration properties of a synthetic montmorillonite compared with a natural Na-exchanged clay analogue. *Applied Clay Sciences*, **48**, 18–25.

Manceau, A., Schlegel, M.L., Nagy, K.L., and Charlet, L. (1999) Evidence of the formation of trioctahedral clay upon sorption of Co^{2+} on quartz. *Journal of Colloid and Interface Science*, **220**, 181–197.

Meunier, A. (2006) Why are clay minerals small? *Clay*

https://doi.org/10.1346/CCMN.2014.0620203 Published online by Cambridge University Press

Minerals, **41**, 551–556.
Meunier, A. (2010) Formation mechanisms of mixed-layer clay minerals. Pp. 53–71 in: *Interstratified Clay Minerals: Origin, Characterization and Geochemical Significance* (S. Fiore, J. Cuadros, and J. Huertas, editors). AIPEA Educational series, Nº**1**.
Michot, L.J. and Villiéras, F. (2002) Assessment of surface energetic heterogeneity of synthetic Na-saponite. The role of layer charge. *Clay Minerals*, **37**, 39–57.
Michot, L.J. and Villiéras, F. (2006) Surface and porosity. Pp. 965–978 in: *Handbook of Clay Science* (F. Bergaya, B.K.G. Theng, and G. Lagaly, Editors). Elsevier, Amsterdam.
Michot, L.J., François, M., and Cases, J.M. (1990) Surface heterogeneity studied by a quasi-equilibrium adsorption procedure. *Langmuir*, **6**, 637–643.
Moll Jr., W.F. (2001) Baseline studies of The Clay Minerals Society Source Clays: geological origins. *Clays and Clay Minerals*, **49**, 374–380.
Moore, D.M. and Reynolds, R.C. (1989) *X-ray Diffraction and the Identification and Analysis of Clay Minerals*. Oxford University Press, New York.
Nakasawa, H., Yamada, H., and Fujita, T. (1992) Crystal synthesis of smectite applying very high pressure and temperature. *Applied Clay Science*, **6**, 395–401.
Peronnet, M., Villiéras, F., Jullien, M., Razafitianamaharavo, A., Raynal, J., and Bonnin D. (2007) Towards a link between the energetic heterogeneities of the edge faces of smectites and their stability in the context of metallic corrosion. *Geochimica et Cosmochimica Acta*, **71**, 1463–1479.
Petit, S., Martin, F., Wiewióra, A., De Perseval, P., and Decarreau, A. (2004) Crystal-chemistry of talc: A near infrared (NIR) spectroscopy study. *American Mineralogist*, **89**, 319–326.
Petit, S., Righi, D., and Decarreau, A. (2008) Transformation of synthetic Zn-stevensite to Zn-talc induced by the Hoffmann-Klemen effect. *Clays and Clay Minerals*, **56**, 645–654.
Rainer, D., Scheidegger, A.M., Manceau, A., Schlegel, M., Baeyens, B., Bradbury, M.H., and Morales, M. (2002) Neoformation of Ni phyllosilicates upon Ni uptake on montmorillonite: a kinetic study by powder and polarized extended X-ray absorption fine structure spectroscopy. *Geochimica et Cosmochimica Acta*, **66**, 2335–2347.
Rudzinski, W., Charmas, R., Piasecki, W., Prélot, B., Thomas, F., Villiéras, F., and Cases, J.M. (1999) Calorimetric effects of simple ion adsorption at silica/ electrolyte interface: A quantitative analysis of surface energetic heterogeneity. *Langmuir*, **15**, 5977–5983.
Sayed Hassan, M., Villiéras, F., Razafitianamaharavo, A., and Michot, L.J. (2005) Geometrical and energetic heterogeneity of kaolinites. The role of exchangeable cations on argon adsorption energy distribution. *Langmuir*, **21**, 12283–12289.
Sayed Hassan, M., Villiéras, F., Gaboriaud, F., and Razafitianamaharavo, A. (2006) AFM and low-pressure argon adsorption analysis of geometrical properties of phyllosilicates. *Journal of Colloid and Interface Science*, **296**, 614–623.
Schlegel, M.L., Manceau, A., Charlet, L., Chateigner, D., and Hazeman, J.L. (2001) Sorption of metal ions on clay minerals. Nucleation and epitaxial growth of Zn phyllosilicate on the edges of hectorite. *Geochimica et Cosmochimica Acta*, **65**, 4155–4170.
Siffert, B. (1962) Quelques réactions de la silice en solution: la fomation des argiles. *Mémoires Service Carte Géologique Alsace Lorraine*, **253**, 142–144.
Środoń, J., Eberl, D.D., and Drits, V.A. (2000) Evolution of fundamental-particle size during illitization of smectite and implications for reaction mechanism. *Clays and Clay Minerals*, **48**, 446– 458.
Sunagawa, I. and Koshino, Y. (1975) Growth spirals on kaolin group minerals. *American Mineralogist*, **60**, 407–412.
Tournassat, C., Neaman, A., Villiéras, F., Bosbach, D., and Charlet, L. (2003) Nano morphology of montmorillonites particles: estimation of the clay edge sorption site density by low-pressure gas adsorption and AFM observations. *American Mineralogist*, **88**, 1989–1995.
Villiéras, F., Cases, J.M., François, M., Michot, L.J., and Thomas, F. (1992) Texture and surface energetic heterogeneity of solids from modeling of low pressure gas adsorption isotherms. *Langmuir*, **8**, 1789–1795.
Villiéras, F., Michot, L.J., Bardot, F., Cases, J.M., François, M., and Rudzinsky, W. (1997a) An improved derivative isotherm summation method to study surface heterogeneity of clay minerals. *Langmuir*, **13**, 1104–1117.
Villiéras, F., Michot, L.J., Cases, J.M., Berend, I., Bardot, F., François, M., Gérard, G., and Yvon, J. (1997b) Static and dynamic studies of the energetic surface heterogeneity of clay minerals. Pp. 573–623 in: *Equilibria and Dynamics of Gas Adsorption on Heterogeneous Solid Surfaces* (W. Rudzinski, W.A. Steele, and G. Zgrablich, editors). Studies in Surface Science and Catalysis, **104**, Elsevier Science Publishers B.V., Amsterdam.
Villiéras, F., Leboda, R., Charmas, B., Bardot, F., Gérard, G., and Rudzinski, W. (1998) High resolution Ar and N_2 assessment of carbosils surface heterogeneity. *Carbon*, **36**, 1501–1510.
Villiéras, F., Michot, L.J., Bardot, F., Chamerois, M., Eypert-Blaison, C., Gérard, G. and Cases, J.M. (2002) Surface heterogeneity of minerals. *Comptes Rendus Geoscience*, **334**, 597–609.
White, G.N. and Zelazny, L.W. (1988) Analysis and implications of the edge structure of dioctahedral phyllosilicates. *Clays and Clay Minerals*, **36**, 141–146.
Zhang, D., Zhou, C., Lin, C., Tong, D., and Yu, W. (2010) Synthesis of clay minerals. *Applied Clay Science*, **50**, 1–11.

(*Received 23 August 2013; revised 30 April 2014; Ms. 702; AE: H. Dong*)

https://doi.org/10.1346/CCMN.2014.0620203 Published online by Cambridge University Press